Theory of light-beam propagation at nonlinear interfaces. I. Equivalent-particle theory for a single interface

A. B. Aceves, J. V. Moloney,* and A. C. Newell
Department of Mathematics, University of Arizona, Tucson, Arizona 85721
(Received 11 August 1988)

A theory is presented that describes the global reflection and transmission characteristics of a self-focused channel propagating at an oblique angle of incidence to an interface separating two or more self-focusing nonlinear dielectric media. The nonlinear wave packet representing the self-focused channel is represented as an equivalent particle moving in an equivalent potential. The dynamics of the particle is described by Newton's equations of motion, with the asymptotic propagation paths of the channel being read off from the associated phase portraits of the equivalent potential. Equilibria of the potential, or equivalently, critical points in the phase plane, represent stationary (stable or unstable) nonlinear surface waves. Stability of the latter follows immediately from a simple inspection of the potential. The shape of the equivalent potential changes with the power in the incident beam. Our theory provides the nonlinear analog of the well-known linear Snell's laws of reflection and transmission. Conditions on the validity of the theory are established in parameter space by extensive numerical solution of the nonlinear partial differential equation describing beam propagation. One important conclusion of the paper is that the predictions of the equivalent-particle theory encompass a wide physical parameter space. As an illustration of an application of the theory, we show how to design an all-optical angle or power adjustable spatial scanning element. Contact is made with earlier numerical studies of beam propagation and nonlinear surface-wave stability at a linear-nonlinear interface.

I. INTRODUCTION

The reflection and transmission characteristics of collimated light beams incident on an interface separating two linear dielectric media, at an angle close to that for total internal reflection, have been the subject of intensive theoretical investigation in recent decades.[1] One important physical manifestation of collimated light reflection, which contrasts with the usual Snell's law predictions for an infinite plane wave, is a finite displacement of the reflected beam from its geometric optics path. This beam displacement, which is referred to as the Goos-Hänchen shift, is of the order of an optical wavelength and has been observed experimentally.[2] The effect can be understood in terms of a Fourier decomposition of the incident linear wave packet representing the collimated optical beam and a careful consideration of the reflection properties of the individual Fourier modes. The nonlinear analogue of this problem has received little attention in the literature with the exception of some numerical studies of the reflection of a Gaussian beam from an interface separating a linear and nonlinear dielectric medium.[3] This latter work established that a nonlinear analogue of the Goos-Hänchen shift could occur and that the shift could be many orders of magnitude greater than the linear one. An explanation for this effect was that the large shift could be attributed to a tendency of the incident beam to remain trapped in the vicinity of a known nonlinear surface wave (NSW) which is intrinsically unstable. A later numerical stability analysis[4] of the known transverse electric (TE) NSW's localized at the interface separating a linear and nonlinear dielectric medium confirmed the existence of stable and unstable stationary NSW's giving support to the conjecture in Ref. 3. With the exception of these two restricted numerical studies, most theoretical investigations in the literature have been concerned with enumerating the various stationary NSW's (Refs. 5-8). A parallel investigation of nonlinear thin-film waveguides has been carried out with the situation being more or less the same as the single interface problem.[5] This latter problem can be distinguished from the single-interface one by the fact that the various permutations and combinations of linear or nonlinear dielectric media lead to the occurrence of a rich spectrum of bifurcating branches of nonlinear solutions at increased incident power. These newly emerging solutions have many properties in common with the single-interface stationary NSW solutions. With only two exceptions,[6,7] the stability of the various branches of nonlinear guided-wave solutions has been confined to numerical beam propagation in a restricted physical parameter range.[8]

In this paper we develop a theory which addresses the propagation of self-focused channels in two or more nonlinear dielectric media. Our basic assumption therefore is that each dielectric has a positive Kerr nonlinear optical coefficient. The theory exploits the fact that the self-focused channels, when localized in a particular medium and well removed from an interface, are spatial solitons of a nonlinear Schrödinger (NLS) equation, whose parameters are appropriate to that particular medium. All of the physically interesting phenomena occur for neighboring dielectrics with small linear refractive-index mismatch so we can assume that the spatial soliton, representing the self-focused channel, will be robust to

perturbations due to the interface. In effect, all of the essential behavior of the incident channel can be captured by allowing the soliton parameters to vary. This assumption is supported by extensive numerical solution of the full beam propagation problem over an extensive region of parameter space. Our theory exploits soliton perturbation techniques first developed by Kaup and Newell[9] and we expect that the conclusions drawn in the present paper should be widely applicable in a number of physical situations where the basic physics is described by an NLS equation with perturbations arising as discontinuities in the material properties. Using the above assumptions we can replace the self-focused channel by a nonlinear wave packet and describe the latters dynamics in terms of the motion of its center of mass and velocity. In this picture, the equivalent particle's velocity is proportional to the sine of the angle of incidence of the incident self-focused channel, its amplitude to the incident power, and its location to the centroid of the channel. The perturbation "felt" by the particle due to the presence of an interface (a neighboring nonlinear medium) causes it to decelerate (bend away) or accelerate (bend towards) as it approaches the interface. The global characteristics of the incident channel's reflection and transmission characteristics at a fixed power, is contained in the associated phase portraits of an appropriate equivalent potential. Moreover, the shape of the equivalent potential is a function of the incident beam power and is captured by two parameters, S, which is the ratio of linear to nonlinear refractive-index mismatches divided by the total power, and α, the ratio of nonlinear Kerr coefficients. These two parameters should be particularly useful in the design of novel all-optical devices. Our theory replaces the rather complex and restrictive numerical beam propagation problem by the much simpler and intuitively appealing Newtonian problem of the motion of an equivalent particle in an equivalent potential. An analytic expression is derived for the nonlinear Goos-Hänchen shift and for the amount of radiation generated due to interaction of the incident channel with the interface. An explicit derivation of the latter is postponed to the second paper of the series, which will be referred to from now on as II. The analytic predictions in all cases are checked by full scale numerical simulations. Stability of earlier known stationary NSW's (Ref. 4) follows trivially as an added bonus of the theory. A main emphasis in II will be to exploit the modular structure of the theory, allowing us to extend it in a standard fashion to the multiple-interface problem where the interface separation exceeds the channels characteristic width. A theory of incident beam breakup into multiple self-focused channels will also be presented in II.

The plan of the present paper is as follows. In Sec. II we review the basic theory illustrating the derivation of the stationary NSW's, which, we shall see later, represent equilibria (stable or unstable) of the equivalent potential or critical points of the associated phase portraits. Contact will be made briefly with known linear theory results. In Sec. III we establish the appropriate scaling for the physical parameters. We find that the problem can be scaled so as to depend on the ratio of three parameters; the incident power to the square root of the linear refractive-index mismatch, the initial velocity (angle of incidence) to the square root of the linear refractive-index mismatch, and the ratio of the nonlinear Kerr coefficients in the neighboring media. An extensive numerical investigation using the beam propagation method shows that the "so-called" nonlinear regime, where the equivalent-particle theory is applicable, spans a wide region of the above parameter space. An important observation in this section is that a hornlike region near the critical angle, where the equivalent-particle theory is expected to breakdown, shrinks very rapidly in size as the nonlinear coefficient ratio decreases from unity (a value of unity representing a uniform background nonlinearity in both neighboring media). In addition, we can provide an analytic expression for one of the boundaries of this region based on the equivalent particle theory derived in the following section. This theory is presented in Sec. IV. For pedagogical purposes we present the theory as a sequence of steps, considering the equivalent particle's motion initially in the separate left and right dielectric media and finally providing a global picture allowing for beam transmission through the interface in either direction. We end Sec. IV with a derivation of a formula for the nonlinear Goos-Hänchen shift. Section V will illustrate a simple application of the equivalent-particle theory in designing a power or angle adjustable all-optical spatial scanner. Contact will also be made in this section of the paper with earlier numerical studies of stability of stationary NSW's at a linear-nonlinear interface[4] and of the reflection and transmission properties of an incident Gaussian beam from such an interface.[3] Section VI will conclude the paper.

II. BASIC THEORY OF BEAM PROPAGATION AND STATIONARY NONLINEAR SURFACE WAVES

The problem of interest involves the propagation of a collimated beam of light in two or more adjoining nonlinear dielectric media. The basic geometry is sketched in Fig. 1, which shows the beam incident at a small angle ψ_i to the interface separating the two neighboring dielectric media; the multiple-interface problem will be dealt with

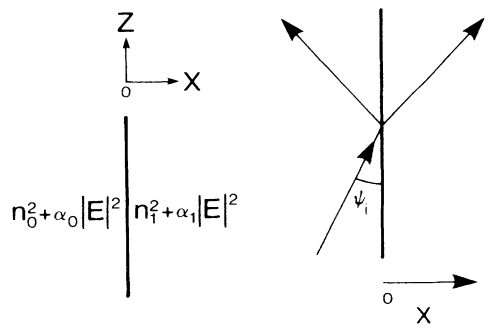

FIG. 1. Schematic representation of the planar waveguide, where we define the angle of incidence ψ_i.

in II. The angle ψ_i is the complement of the usual angle of incidence in Snell's laws and will be small due to the assumed smallness of the linear refractive-index jump across the interface. The squared refractive index in each medium is assumed to be of the Kerr type, $n^2(x,|E|^2)=n_0^2+\alpha_0|E|^2$, $x<0$; $n^2(x,|E|^2)=n_1^2+\alpha_1|E|^2$, $x>0$, where $n_0>n_1$ and $0<\alpha_0\leq\alpha_1$ in order to ensure the existence of stationary trapped surface waves. The light channel will propagate close to the z axis and will be bounded in the transverse x dimension. We anticipate that the light channel may be reflected by or transmitted through the interface at $x=0$. Trapped stationary NSW's where the envelope of the TE nonlinear wave is z independent may also exist above a threshold power level. Our aim is to develop a self-contained theory that predicts accurately the final large z asymptotic state of the incident beam over a wide range of physical parameter space, as a function of incident angle or power variation.

The propagation of a TE wave in the x-z plane is described by the scalar wave equation,

$$\frac{\partial^2 E}{\partial z^2}+\frac{\partial^2 E}{\partial x^2}=-n^2k_0^2E\ , \tag{1}$$

where k_0 is the free-space wave number. Plane-wave solutions of (1),

$$E=\exp[i(k_z z+k_x x]\ ,$$

satisfy the following dispersion relation:

$$k_z^2+k_x^2=n^2k_0^2\ . \tag{2}$$

Making the ansatz $E(x,z)=F(x,z)\exp(i\beta k_0 z)$ in Eq. (1) and assuming paraxial rays, we obtain the following propagation equation for the slowly varying envelope $F(x,z)$ of the optical field:

$$2i\beta k\frac{\partial F}{\partial z}+\frac{\partial^2 F}{\partial x^2}-(\beta^2-n^2)k^2F=0\ .$$

Making the change of variables $x'=kx$, $z'=kz$ and dropping the primes we obtain the dimensionless form

$$2i\beta\frac{\partial F}{\partial z}+\frac{\partial^2 F}{\partial x^2}-(\beta^2-n^2)F=0\ . \tag{3}$$

The continuity of tangential components of the electric and magnetic fields at the interface translates into continuity of F and F_x across the interface for TE waves. For bounded solutions localized near the interface, we also require that F and $F_x\to 0$ as $x\to\pm\infty$.

A. Linear theory

A brief overview will be given now of the linear theory of a collimated beam incident on an interface separating two linear dielectric media, at an angle close to that for total internal reflection. This problem turns out to be more complicated than the nonlinear one and a considerable literature exists[1] on calculations of the Goos-Hänchen shift. An asymptotic estimate of the power carried in the reflected beam will be computed in order to compare with the nonlinear theory which is the central focus of this paper. We will not be concerned with computations of the Goos-Hänchen shift for this problem. Consider the broad incident, reflected and transmitted beams (wave packets) as being superpositions of plane waves. The problem then translates into finding, for each Fourier component of the incident wave packet, and amplitudes of the corresponding reflected and transmitted components. Assume an incident plane wave whose x wave number is k_x; then the field in the left-hand medium will be

$$F_{\text{left}}=\exp\left[i\left[k_x x+\frac{k_z z}{2\beta}\right]\right]+R(k_x)\exp\left[-i\left[k_x x-\frac{k_z z}{2\beta}\right]\right]\ , \tag{4}$$

where the first term represents the incoming wave and the second term is the outgoing reflected wave. Similarly, the field in the right-hand medium is

$$F_{\text{right}}=T(k_x)\exp\left[i\left[k_x' x-\frac{k_z z}{2\beta}\right]\right]\ . \tag{5}$$

Direct substitution of (4) and (5) in Eq. (3) with $\alpha_0=\alpha_1=0$ determines the dispersion relation for the two media

$$k_z=-k_x^2-(\beta^2-n_0^2)\ ,$$
$$k_z=-(k_x')^2-(\beta^2-n_1^2)\ ,$$

from which one finds that $(k_x')^2=k_x^2-(n_0^2-n_1^2)$, which is simply Snell's law. Note that these expressions follow by expanding Eq. (2) and dropping terms proportional to k_z^2 consistent with the paraxial ray approximation. To determine $R(k_x)$ and $T(k_x)$ one imposes the continuity conditions of F and dF/dx valid for transverse electric fields. One obtains the Fresnel formulas,

$$R(\bar{k}_x)=\frac{\bar{k}_x-(k_x^2-1)^{1/2}}{\bar{k}_x+(k_x^2-1)^{1/2}}\ ,$$
$$T(\bar{k}_x)=\frac{2\bar{k}_x}{\bar{k}_x+(\bar{k}_x^2-1)^{1/2}}\ ,$$

where $\bar{k}_x=k_x/\sqrt{\Delta}$, $\Delta=n_0^2-n_1^2>0$.

These results allow us to find integral expressions for the fields in both media when the incident field is a wave packet; for this case,

$$F_{\text{left}}=\int_{-\infty}^{\infty}A(k_x)\exp\left[i\left[k_x x+\frac{k_z z}{2\beta}\right]\right]dk_x+\int_{-\infty}^{\infty}R(k_x)A(k_x)\exp\left[-i\left[k_x x-\frac{k_z z}{2\beta}\right]\right]dk_x \tag{6}$$

and

$$F_{\text{right}}=\int_{-\infty}^{\infty} T(k_x)A(k_x)\exp\left[i\left[k_x'x+\frac{k_z z}{2\beta}\right]\right]dk_x \ , \tag{7}$$

respectively, where $A(k_x)$ in the Fourier transform of the incoming wave packet. Since we cannot evaluate the integrals in terms of elementary functions we will look for an asymptotic expansion for each component of the field for large values of z. The leading-order term in an asymptotic expansion of the reflected component for an incoming sech-like wave packet can be computed in a straightforward fashion. Let the incoming wave packet be

$$F_{\text{in}}=E_0\,\text{sech}[2\eta(x-\bar{x})]e^{i(v/2)x} \ ,$$

where $\bar{x}\ll 0$ and of width $\eta^{-1}\gg 1$. Then its Fourier transform is

$$A(k_x)=\frac{E_0}{4\eta}\text{sech}\left[\frac{\pi}{4\eta}\left[k_x-\frac{v}{2}\right]\right]e^{i(v/2-k_x)\bar{x}} \ .$$

Observe that since F_{in} is broad, $A(k_x)$ is very narrow with its peak located at $k_x=v/2$. We now find the leading-order term of the asymptotic expansion for large z of the second term in (6) using the stationary-phase method. It is

$$\int_{-\infty}^{\infty} R(\bar{k}_x)A(k_x)\exp\left[i\left[k_x x+\frac{k_z z}{2\beta}\right]\right]dk_x \sim \frac{R\left[\frac{v}{2\sqrt{\Delta}}\right]}{4\eta}\left[\frac{2\beta\pi}{z}\right]^{1/2}E_0\,\text{sech}\left[\frac{\pi\beta\left[x+\bar{x}+\frac{vz}{2\beta}\right]}{4\eta z}\right]e^{i\phi} \ , \tag{8}$$

where

$$\phi=(\beta^2-n_0^2)\frac{z}{2\beta}-\frac{(x+\bar{x})^2}{4z} \ .$$

In (8) we approximate $R(-\beta(x+\bar{x})/\sqrt{\Delta}z)\sim R(v/2\sqrt{\Delta})$ which is the first term of its Taylor expansion. Therefore, if we call the reflected field given by (8) F_r, it follows that

$$\int_{-\infty}^{\infty}|F_r|^2dx=\left|R\left[\frac{v}{2\sqrt{\Delta}}\right]\right|^2\int_{-\infty}^{\infty}|F_{\text{in}}|^2dx \ . \tag{9}$$

The portion of the incident power being reflected by an interface between two linear dielectrics when the incoming wave packet is broad is given by the Fresnel formula evaluated at $\bar{k}_x=v/2\sqrt{\Delta}$. One can now conclude that in this case, there is total internal reflection if $v/2\sqrt{\Delta}<1$; otherwise there is partial reflection and partial transmission. Thus the critical angle ψ_i is $\psi_{i\,\text{crit}}=\sin^{-1}(2\sqrt{\Delta})$.

The leading-order term of the reflected field (8) is the geometrical optics component. If one describes beams of light as rays, then the incident beam is a ray given by the equation $x=\bar{x}+vz$. The reflected ray is given by the equation, $x=-\bar{x}-vz$, and the two rays will intersect at the interface. The reflection coefficient given by Eq. (8) will be compared with the corresponding one for the nonlinear problem in Sec. III B. The linear Goos-Hänchen shift appears as a correction to the reflected field F_r obtained by going to the next-order term of its expansion where one must consider the branch points of $R(\bar{k}_x)$. Relevant recent work in this area is given in Ref. 1.

B. Stationary nonlinear surface waves

This subsection will illustrate how one computes the z-independent stationary TE NSW's at the interface separating two nonlinear dielectric media with positive Kerr coefficients. As remarked earlier in the Introduction, these solutions will represent equilibrium points of our equivalent potential or critical points of its associated phase portraits. An extensive literature exists on the enumeration of such nonlinear stationary surface- and guided-wave solutions for both TE and TM waves.[10] At the end of this subsection we will present the stationary NSW solutions for a linear-nonlinear interface. These follow as a special limit of the more general solutions derived below.

If the envelope of the wave F is independent of the direction of propagation z, then it must satisfy the equation

$$\frac{d^2F(x)}{dx^2}[\beta^2-n^2(x,|F|^2)]F(x)=0 \ . \tag{10}$$

For a given β a solution of (10) is given by

$$F^+(x)=\begin{cases}\left[\frac{2(\beta^2-n_0^2)}{\alpha_0}\right]^{1/2}\text{sech}[(\beta^2-n_0^2)^{1/2}(x-x_0)] \ , & x<0\\ \left[\frac{2(\beta^2-n_1^2)}{\alpha_1}\right]^{1/2}\text{sech}[(\beta^2-n_1^2)^{1/2}(x-x_1)] \ , & x>0 \ .\end{cases} \tag{11}$$

A necessary condition for the existence of these solutions is that $\beta^2>n_0^2$. The three free parameters β, x_0, and x_1 are determined from the continuity of $F(x)$ and $F_x(x)$ for the TE wave at the interface. The two equations for x_0, x_1 are

$$\left[\frac{2(\beta^2-n_0^2)}{\alpha_0}\right]^{1/2}\operatorname{sech}[(\beta^2-n_0^2)^{1/2}x_0]$$
$$=\left[\frac{2(\beta^2-n_1^2}{\alpha_1}\right]^{1/2}\operatorname{sech}[(\beta^2-n_1^2)^{1/2}x_1] \quad (12)$$

and

$$(\beta^2-n_0^2)^{1/2}\tanh(\beta^2-n_0^2)x_0$$
$$=(\beta^2-n_1^2)^{1/2}\tanh[(\beta^2-n_1^2)^{1/2}x_1]\ . \quad (13)$$

Solving for x_0, x_1 we find that

$$x_0=\frac{1}{2(\beta^2-n_0^2)^{1/2}}\ln\frac{1+r(1-\mu^2)^{1/2}}{1-r(1-\mu^2)^{1/2}}\ , \quad (14)$$

$$x_1=\frac{1}{2(\beta^2-n_1^2)^{1/2}}\ln\frac{1+(1-\mu^2)^{1/2}}{1-(1-\mu^2)^{1/2}}\ , \quad (15)$$

where $\mu^2=(n_0^2-n_1^2)/[(1-\alpha)(\beta^2-n_1^2)]$ must be less than 1 in order to have real solutions, and $r=[(\beta^2-n_1^2)/(\beta^2-n_0^2)]^{1/2}$. The condition $\mu^2<1$ implies a condition on β, namely,

$$\beta^2>\beta_{\min}^2=n_1^2+\frac{\Delta}{1-\alpha}>n_0^2\ .$$

These solutions which we refer to as $F^+(x)$, correspond to wave packets whose envelope has a peak at $x_1>0$. However, observe from (12) and (13) that if x_0 and x_1 satisfy these equations, so also do $-x_0$ and $-x_1$. Therefore there is a dual family of steady-state solutions,

$$F^-(x)=\begin{cases}\left[\dfrac{2(\beta^2-n_0^2)^{1/2}}{\alpha_0}\right]\operatorname{sech}[(\beta^2-n_0^2)^{1/2}(x+x_0)], & x<0\\ \left[\dfrac{2(\beta^2-n_1^2)^{1/2}}{\alpha_1}\right]\operatorname{sech}[(\beta^2-n_1^2)^{1/2}(x+x_1)], & 0<x\end{cases} \quad (16)$$

where now the peak of $F^-(x)$ is at $x=-x_0<0$. Typical plots of F^+ and F^- are shown in Fig. 2.

The power $P^{\pm}=\int_{-\infty}^{\infty}|F^{\pm}(x)|^2dx$ corresponding to these solutions is given by

$$P^{\pm}=2\left[\frac{(\beta^2-n_0^2)^{1/2}}{\alpha_0}+\frac{(\beta^2-n_1^2)^{1/2}}{\alpha_1}+\left[\frac{1}{\alpha_1}\pm\frac{1}{\alpha_0}\right]\left[\beta^2-n_1^2-\frac{\Delta}{1-\alpha}\right]^{1/2}\right]\ . \quad (17)$$

In Fig. 3, we plot β versus P for the case $\alpha=0.25$, where the branch $ABCD$ corresponds to P^+ and the branch DE to P^-. We note that $\beta_{\min}$ corresponds to the value of β where $F^+(x)=F^-(x)$, or where $x_0=x_1=0$, and that there is a critical power P_C below which no steady-state solutions exists. Also plotted in Fig. 3 is the corresponding $\bar{x}$ versus P graph, where $\bar{x}$ is the position of the peak of the steady-state solution; that is, $\bar{x}=x_1$ for $F^+(x)$ and $\bar{x}=x_0$ for $F^-(x)$. We label the branches the same way as in the β versus P graph.

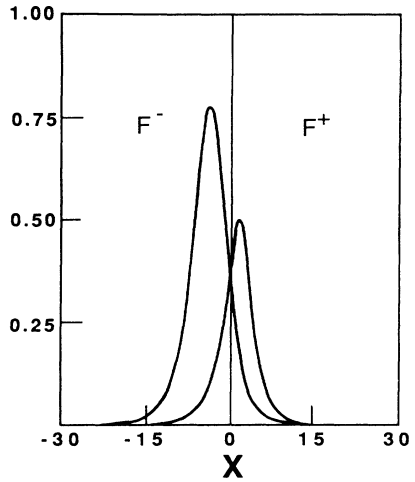

FIG. 2. Plots of $F^+(x)$ and $F^-(x)$ for values of $\alpha_0=0.5$, $\alpha_1=2.0$, $n_0^2=0.11$, $n_1^2=0.01$, and $\beta=0.7$.

The above stationary analysis does not address the important question of stability of these NSW's. By stability, we simply mean that, assuming that we can couple such a wave to the interface, it will remain localized at the latter as it propagates. The general question of the stability of nonlinear surface and guided waves is complicated and much of the analysis to date has been numerical, involving use of the beam propagation method to launch the stationary NSW's or NGW's at various points on the P versus β characteristic curves.[4,6,8] This approach is of limited use, requiring heavy computational effort in a narrow physical parameter window. The first analytic stability result for a certain class of nonlinear guided waves based on a topological argument[6] has been confirmed numerically by a number of authors. A more recent work has extended the analytic stability predictions to a wider class of NGW solutions.[7] The equivalent particle picture, in addition to giving quantitative insight into the global beam reflection and transmission properties, will provide the stability properties of the stationary NSW solution branches of the P versus β characteristic in Fig. 3, automatically. We will show that the branch ABC is stable and that the branch CDE is unstable even though, in this case, $\partial P/\partial\beta>0$ along DE. This means that the stability criterion suggested in Ref. 4 that P increasing (decreasing) with respect to β infers stability (instability) is not true in general. It is, however, true in the particular situation of the linear-nonlinear problem. Also, we notice that the stable solutions occur only when the peak is in the medium with the higher nonlinear refractive index α_1.

We conclude this section by showing that one can recover the steady-state solutions of the linear-nonlinear case given in Ref. 10 by taking the limit $\alpha=0$ in $F^+(x)$. For $x>0$,

$$\lim_{\alpha_0\to 0}F^+(x)=\left[\frac{2(\beta^2-n_1^2}{\alpha_1}\right]^{1/2}\times\operatorname{sech}[(\beta^2-n_1^2)^{1/2}(x-x_1)]\ , \quad (18)$$

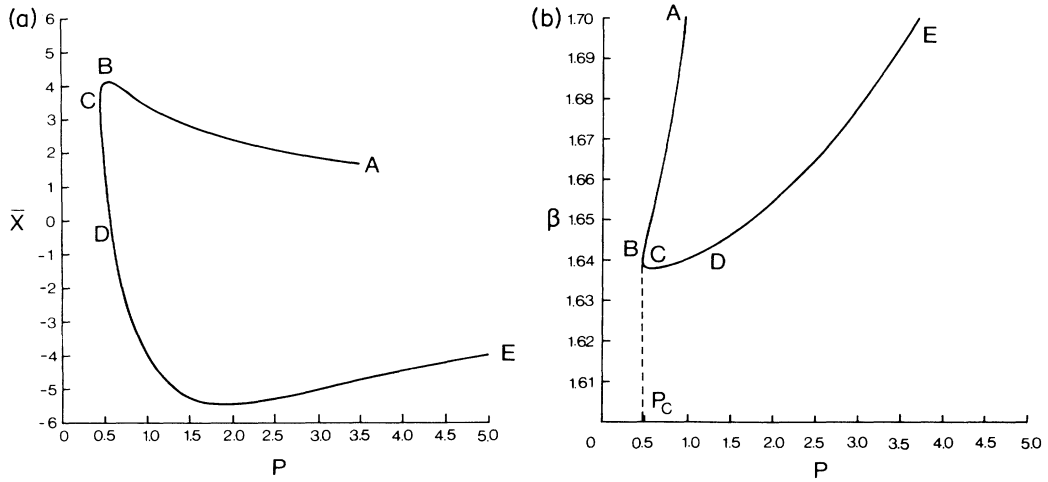

FIG. 3. Plots of $\bar{x}$ vs P and β vs P for $\alpha=0.25$. Branch $ABCD$ corresponds to F^+ solutions, and branch DE to F^-. Branch ABC is stable and branch CDE is unstable.

with

$$x_1=\frac{1}{2(\beta^2-n_1^2)^{1/2}}\ln\frac{(\beta^2-n_1^2)^{1/2}+(\beta^2-n_0^2)^{1/2}}{(\beta^2-n_1^2)^{1/2}-(\beta^2-n_0^2)^{1/2}} . \tag{19}$$

For $x<0$,

$$\lim_{\alpha_0\to 0}F^+(x)=\left[\frac{2(n_0^2-n_1^2}{\alpha_1}\right]^{1/2}\exp[(\beta^2-n_0^2)^{1/2}x] , \tag{20}$$

which is found from the limit of Eq. (14) as $\alpha_0\to 0$ using the fact that

$$\lim_{\alpha_0\to 0}\frac{1}{\sqrt{a_0}}\exp[-(\beta^2-n_0^2)^{1/2}x_0]=\left[\frac{\Delta}{4\alpha_1(\beta^2-n_0^2)}\right]^{1/2} .$$

Equations (18)–(20) are the solutions of the linear-nonlinear case.[4] For this case $\lim_{\alpha_0\to 0}P_D=\infty$, in agreement with the fact that all steady-state solutions of the linear-nonlinear case have their peak at positive x. This fact is obvious once we observe that since Eq. (3) in the linear case is purely dispersive, an initial wave packet propagating in such medium will always spread, losing its original shape. The infinite-power solution at P_D corresponds to the infinite-plane-wave case studied in Ref. 11. Figures 4(a) and 4(b) show, respectively, the β versus P and $\bar{x}$ versus P plots for the case $\alpha=0$. The stability of these solutions will also be discussed in Sec. IV.

III. PARAMETER-SPACE CHARACTERIZATION OF GLOBAL PROPAGATION EFFECTS

This section is devoted to two important tasks. First, we scale the propagation equation (3) so as to isolate the important physical parameters of the problem. This scaled problem is investigated numerically, using the beam propagation method, in order to infer the global reflection and transmission properties of an incident collimated optical beam under a wide variety of initial conditions. As in the linear case of Sec. II, we will restrict the analysis to incoming wave packets that have sech-like shapes. Since the equation in the left-hand medium is nonlinear Schrödinger, there exists a large class of initial profiles that will decompose into a sech-like (spatial soliton) profile and some radiation before encountering the interface. The Appendix reviews the beam propagation

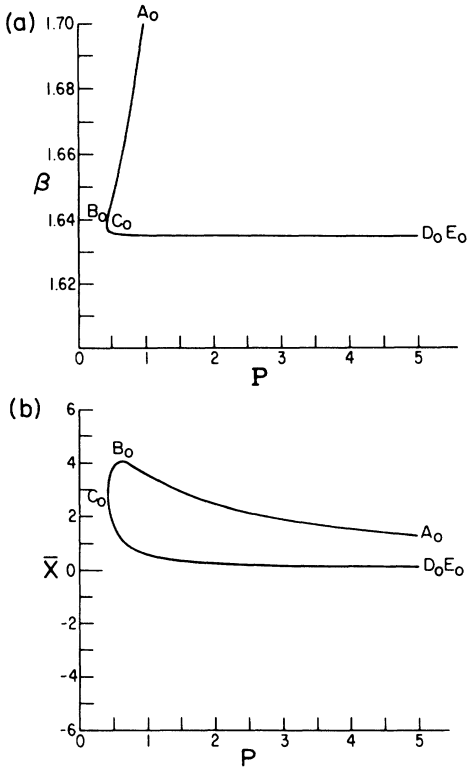

FIG. 4. Plots of β vs P and $\bar{x}$ vs P for $\alpha=0$. The $A_0B_0C_0$ branch is stable and the $C_0D_0E_0$ branch is unstable.

numerical technique used in the present work. In practice, we solve Eq. (3) for different combinations of left- and right-hand medium physical parameters in order to confirm the validity of our scaling laws.

A. Scaling of the beam propagation equation

The parameters of this problem are the linear and nonlinear refractive indexes of the two media ($n_i^2,\alpha_i,i=0,1$), and the parameters of the incident wave packet, its power ($\int_{-\infty}^{\infty}|F|^2dx$) and angle of incidence. In total we have six parameters and the purpose of this section is to find appropriate relations between them that can give us a full characterization of the problem with as few parameters as possible. We will obtain the reduced parameter space from the proper choice of rescalings and transformations on the field and the beam propagation equation.

Consider the following set of transformations:

$$F(x,z)=\left[\frac{2\Delta}{\alpha_0}\right]^{1/2}F'(x',z')e^{i(\beta^2-n_0^2)z/(2\beta)},$$

where

$$x'=\sqrt{\Delta}x,\quad z'=\frac{\Delta z}{2\beta},$$

then $F'(x',z')$ satisfies

$$i\frac{\partial F'}{\partial z'}+\frac{\partial^2 F'}{\partial x'^2}+2|F'|^2F'=\begin{cases}0, & x<0\\ F'-2(\alpha^{-1}-1)|F'|^2F', & x>0\end{cases}$$

that is, the equation for F' has only one parameter α. Now, if the initial wave packet $F(x,0)$ has the form of an exact soliton traveling in the left-hand medium,

$$F(x,0)=2/\alpha_0 2\eta_0\,\mathrm{sech}\,2\eta_0(x-\bar{x}_0)e^{iv_0x/2},$$

then

$$F'(x',0)=\frac{2\eta_0}{\sqrt{\Delta}}\,\mathrm{sech}\frac{2\eta_0(x'-\bar{x}'_0)}{\sqrt{\Delta}}e^{iv_0x'/2\sqrt{\Delta}}.$$

What this means is that for a fixed value of α all initial conditions with the same values of $\eta_0/\sqrt{\Delta}$ and $v_0/\sqrt{\Delta}$ will show the same behavior except for a multiplicative constant $\sqrt{2/\alpha_0}$ of their respective amplitudes. Since we will characterize the different behaviors in parameter space in terms of the ratio of reflected to incident power, this constant is not relevant to the analysis. Now that we have been able to reduce the number of parameters to 3 we will map out in this parameter space, the regimes of different behavior of an incident sech-like wave packet at an interface between two nonlinear dielectrics.

B. Parameter-space representation

In order to obtain a detailed picture in parameter space we performed an extensive numerical analysis covering a wide range of parameters. In each case studied, the amount of power reflected was measured from the numerical simulation and the asymptotic state of the field was established.

We have observed three different regimes in each $\alpha=$const plane that we shall define as linear, intermediate, and the strongly nonlinear. The linear regime is found for small values of $\eta_0/\sqrt{\Delta}$ (less than 0.05 in all cases), that is, when the incident wave packet is broad. Here the evolution of the wave packet as well as the amount of power being reflected was insensitive to α. Furthermore, the way the wave packet is distorted at the interface before it splits into a reflected and a transmitted component is very reminiscent of the linear case; that is, we see an interference pattern at the interface that creates two dispersive waves: one is transmitted and the other is reflected [see Fig. 5(a)]. The reflection coefficient follows very closely that of the linear case obtained in Sec. III A, as we can observe in Fig. 6(a), where we compare $|R(v_0/\sqrt{\Delta})|^2$ given by the Fresnel formula with the numerical measurements obtained for $\eta_0/\sqrt{\Delta}=0.05$ and $\alpha=1$. Recall that the results are insensitive to the magnitude of α in this regime.

Once we start increasing the parameter η_0/Δ, the behavior is no longer linear. Instead we still see two different behaviors which we define as intermediate and the strongly nonlinear. The equivalent-particle theory

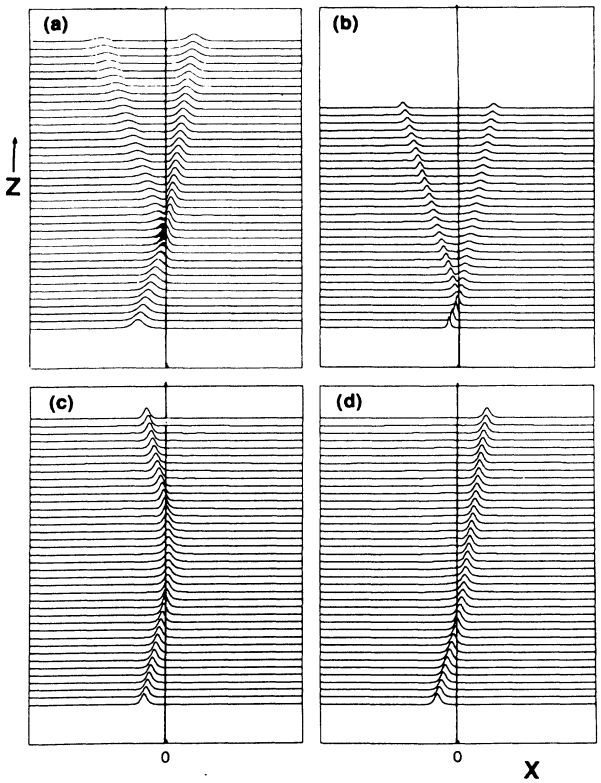

FIG. 5. Evolution of an incident wave packet for three different values of η_0/Δ: (a) 0.05, (b) 0.3, (c) and (d) 0.8. In (a)–(c), $v_0/\sqrt{\Delta}=1.9$, which is below the critical angle of total reflection ($v_0/\sqrt{\Delta}=2$); and in (d), $v_0/\sqrt{\Delta}=2.2$. In all cases $\alpha=1.0$.

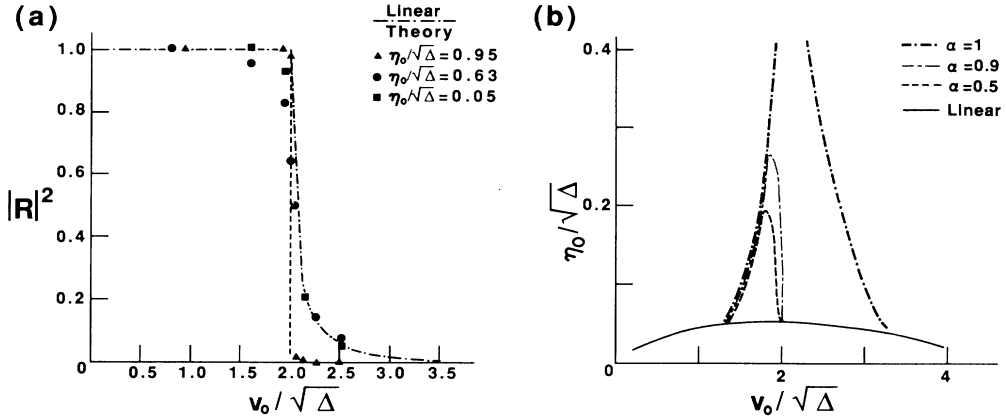

FIG. 6. Plots of (a) the reflection coefficient $|R|^2$ vs scaled incident angle $v_0/\sqrt{\Delta}$ for $\alpha=1.0$. Three cases corresponding to different $\eta_0/\sqrt{\Delta}$ are shown. The dashed curve is the Fresnel formula for linear reflection of a plane wave. (b) $(\eta_0/\sqrt{\Delta}, v_0/\sqrt{\Delta})$ parameter-space representation of the linear, intermediate, and nonlinear regimes for three different values of α, 1.0, 0.9, and 0.5.

developed in Sec. IV is valid in the nonlinear regime. Our immediate objective now is to specify both numerically and analytically the boundaries separating this regime from the intermediate one. To achieve this, we numerically solve (3) for a given initial wave packet, whose width η_0^{-1} is narrow enough that it lies outside the linear regime. In order to understand what characterizes the nonlinear regime for different values of the parameters, it is necessary to present here some of the predictions that will be proved and explained in detail in Sec. IV.

We begin by considering the case $\alpha > \frac{4}{9}$, since for these values of α the equivalent-particle theory predicts that in the strongly nonlinear regime a single wave packet prevails with very small losses in radiation [of the order of $(1-\sqrt{\alpha})^2$] whenever it crosses the interface. Also a new relation between the parameters $S_0=1/4(\eta_0/\sqrt{\Delta})^2(1-\alpha)$, will play an important role in the global dynamics and, in particular, it gives an explicit relation, for a fixed α, between $\eta_0/\sqrt{\Delta}$ and $v_0/\sqrt{\Delta}$ that separates the cases of total reflection from those of total transmission, whenever $S_0 > \max(1/\alpha, 2/3\alpha^2)$. The expression is

$$\frac{4(1-\alpha^2)(\eta_0/\sqrt{\Delta})^2}{3\alpha^2}+\frac{(v_0/\sqrt{\Delta})^2}{4}=1\ . \tag{21}$$

This represents an ellipse in the $(\eta_0/\sqrt{\Delta}, v_0/\sqrt{\Delta})$ plane, and we will now see that a section of it defines one of the boundaries of separation between the intermediate and the strongly nonlinear regimes.

From our numerical analysis we were able to conclude that if $\alpha < 1$, a beam that crosses the interface from left to right always behaves as predicted by the strongly nonlinear theory. That is, it loses a very small amount of power into radiation and instead the wave packet initially narrows as it crosses the interface. This is intuitively clear since the wave packet is now in a medium with a higher nonlinearity so that the focusing effect is more prominent. If the wave packet was reflected and crossed the interface going again to the left-hand medium, we observed in some, but not all cases, a significant change in the original wave packet. In some instances *bigger* losses of power into radiation or even soliton breakup were evident, both being contrary to the predictions given by the strongly nonlinear theory. Details of these phenomena are postponed to II.

The above observations mean that for $\frac{4}{9} < \alpha < 1$, and $\eta_0/\sqrt{\Delta} > 0.05$, if $v/\sqrt{\Delta}$ is such that the wave packet is transmitted, the behavior is consistent with being in the nonlinear regime. This means that one of the boundaries that separates the intermediate from the strongly nonlinear regimes has an analytical expression given, for each α, by Eq. (21). If, on the other hand, the angle of incidence (proportional to v) is small enough so that the peak of the wave packet does not cross the interface, once again the equivalent-particle dynamics prevails, consistent with strongly nonlinear behavior. Therefore we expect a second boundary to the left of the section of the ellipse represented by Eq. (21). We found no analytical expression for this boundary. Instead, we inferred its form from the numerical simulations. It is important to mention that this latter boundary as well as the boundary separating the linear from the nonlinear regimes were constructed from the numerical simulations. Our numerics confirms the analytic prediction for the right-hand boundary when $\alpha < 1$. We observe in practice that all transitions, whether from the linear to nonlinear or from the intermediate to the strongly nonlinear regimes were very sharp. The boundary separating the linear from other regimes is consistent with an asymptotic estimate, which is not given here. Finally we observed that, except for the case $\alpha=1$, both boundaries separating the intermediate from the strongly nonlinear regimes intersect at a finite value of $\eta_0/\sqrt{\Delta}$. That is, for every α bigger than $\frac{4}{9}$, there is a critical $\eta_0/\sqrt{\Delta}$, that depends on α, above which the strongly nonlinear regime prevails for all angles of incidence.

Figure 6(b) shows the three regimes for three values of α, 1.0, 0.9, and 0.5 where we see that as α decreases the

nonlinear regime becomes more dominant. It is interesting to observe that the value of S at the intersection point of the two boundaries was found to be always close to 4 for all the different values α's that were studied. This suggests the possibility of defining the corners by the condition

$$\frac{1}{4(\eta_0/\sqrt{\Delta})^2(1-\alpha)}=4 .$$

This defines the maximum value of $\eta_0/\sqrt{\Delta}$ for which the intermediate regime can exist; it is

$$\left[\frac{\eta_0}{\sqrt{\Delta}}\right]^2_{\max}=\frac{1}{16(1-\alpha)} .$$

Note that $(\eta_0/\sqrt{\Delta})^2_{\max}\to\infty$ as $\alpha\to 1$, consistent with the numerically observed fact that for the $\alpha=1$ case, the intermediate regime extends to all possible values of $(\eta_0/\sqrt{\Delta})^2$, albeit in an ever decreasing velocity (angular) window about critical $v_0/\sqrt{\Delta}=2$. An explanation of this phenomenon could be that, for this case, the lack of self-focusing action associated with a larger nonlinear coefficient in the right-hand (or left-hand) medium means that the incoming wave packet "feels" the full impact of the perturbation due to the linear discontinuity in refractive indexes. Consequently, more incident power may be converted into radiation or even lead to breakup at the first crossing of the interface, contrary to the $\alpha<1$ case. In this special case we observe that, even for transmitted wave packets, losses in power not predicted by the nonlinear theory were always observed [see Fig. 5(b)]. However, as $\eta_0/\sqrt{\Delta}$ increases, the nonlinear regime dominates, and then we see, for the $\alpha=1$ case, either total reflection [Fig. 5(c)] or total transmission [Fig. 5(d)].

If $\alpha<\frac{4}{9}$, we will see in II how the description of the nonlinear regime becomes slightly more complicated because, for these values of α, the transmitted wave packet will split into several soliton components in the right-hand medium. Each soliton will then evolve separately and, in some cases one of the new wave packets may be reflected back to the left-hand medium. In this case the asymptotic state will consist of several soliton components, some transmitted, some reflected, and radiation. Here, we have not found explicit boundaries separating the different regimes, although we can say that the behavior described here and explained in more detail in II is a good approximation of the true behavior for a wide range of parameters (see, for example, Table I).

Our extensive numerical study in this section has established the existence of three distinct regimes of behavior in $[\eta_0/\sqrt{(\Delta)},v_0/\sqrt{(\Delta)}]$-parameter space. For broad incident channels $[\eta_0/\sqrt{(\Delta)}<0.05]$ the reflection and transmission behavior is insensitive to the magnitude of α and identical to that of a linear wave packet. As the reflected or transmitted components depart from the interface they gradually disperse as expected for linearly diffracting waves. In the intermediate regime, when near the critical angle, the incident channel again splits into a partially reflected and a partially transmitted component. Now, however, each component may remain as a localized self-focused channel (spatial soliton). A full analysis of this regime should include equations of evolution for the continuous spectrum of the linear eigenvalue problem associated with NLS [see Eq. (A1) of II], since what we observe is that, at the interface, the perturbation excites other nonlinear modes instead of only perturbing the parameters of the incoming soliton. In the fully nonlinear regime, the incident channel is either totally reflected or transmitted as it is tuned through the critical angle. The finite amount of radiation generated due to interaction with the interface can be accurately estimated as we shall see in Sec. IV. This latter regime is the focus of the rest of the paper.

TABLE I. List of the relevant parameters of the problem. A fourth parameter $S_0=4/(\eta_0/\sqrt{\Delta})^2(1-\alpha)$ will also play an important role in the equivalent-particle theory.

Nondimensional power	$\eta_0/\sqrt{\Delta}$
Nondimensional angle	$v_0/\sqrt{\Delta}$
Ratio of nonlinear refractive-index coefficients	α

IV. EQUIVALENT-PARTICLE THEORY

This section presents the main result of our paper. For pedagogical purposes, we develop the equivalent-particle theory in a series of steps. First, we consider the case where the peak of the wave packet stays on one side of the interface for all time. In this situation, the discontinuity at the interface acts as a finite, uniformly small perturbation, on the tail of the beam. This interaction, in turn, can cause the incident self-focused channel to bend away from interface. The equivalent-particle picture will allow us to monitor the channel peak intensity location as either the incident angle or power are varied. A similar development follows automatically for the wave packet restricted to the right-hand medium. The final step will be to allow for transmission through the interface from left to right or vice versa. The end result will be a theory which replaces the computationally intensive and restrictive beam propagation method by the simple and intuitively appealing problem of the motion of an equivalent particle in an equivalent potential. In other words, the global characteristics of beam propagation near an interface reduce to studying Newton's equations of motion. The beam propagation method will be used to check the accuracy of the theoretical trajectories. The theory will also indicate under which conditions a wave packet approaching the interface will cross it.

A. Self-focused channel in the left-hand medium

Suppose that a single wavepacket evolves in z such that its peak always remains in the left-hand medium. It will soon be clear what this assumption means in terms of the shape of the envelope F of the TE field.

Let

$$F(x,z)=\left[\frac{2}{\alpha_0}\right]^{1/2}A(x,\tau)e^{i(\beta^2-n_0^2)z/(2\beta)},$$

where $\tau=z/2\beta$, whence $A(x,\tau)$ satisfies

$$i\frac{\partial A}{\partial\tau}+\frac{\partial^2 A}{\partial x^2}+2|A|^2A=VA\ . \tag{22}$$

The perturbation potential V is

$$V=\begin{cases}0, & x<0\\ \Delta-2[\alpha^{-1}-1]|A|^2, & x>0\end{cases} \tag{23}$$

where $\Delta=n_0^2-n_1^2$. We now see that by defining F and τ as is done here the $A(x,\tau)$ satisfies the NLS equation with an extra term on the right-hand side. In the absence of an interface, $\alpha=1$, $\Delta=0$ and therefore $V\equiv 0$. In that case it is well known that the general solution will consist of soliton and nonsoliton components. The amount of each can be determined from $A(x,0)$ using inverse scattering theory. Given (22), it is easy to write the following exact expressions for the rate of change of the normalized dimensionless power:

$$p=\int_{-\infty}^{\infty}AA^*dx$$

(the total power $P=\int_{-\infty}^{\infty}FF^*dx=2p/\alpha_0$), the average position

$$\bar{x}=p^{-1}\int_{-\infty}^{\infty}xAA^*dx\ ,$$

and the average velocity

$$v=ip^{-1}\int_{-\infty}^{\infty}\left[A\frac{\partial A^*}{\partial x}-A^*\frac{\partial A}{\partial x}\right]dx$$

of the normalized field $A(x,\tau)$.

We obtain

$$\frac{dp}{d\tau}=0\ , \tag{24a}$$

$$\frac{d\bar{x}}{d\tau}=v\ , \tag{24b}$$

$$\frac{dv}{d\tau}=-2p^{-1}\int_{-\infty}^{\infty}\frac{\partial V}{\partial x}AA^*dx\ . \tag{24c}$$

These expressions are exact and involve no approximation. The equivalent-particle description is obtained by making the assumption that the field moves collectively, in the sense that its local intensity AA^* is a function only of $x-\bar{x}(\tau)$. The motivation for this approximation is as follows. An arbitrary wave packet, initially a long way from the interface, will break up into soliton, multisoliton, and radiation components and the interaction of these different components can be treated separately. For simplicity, we are always going to assume that the incoming wave packet is a single soliton for the medium in which it initially travels, which for the moment is the left-hand medium,

$$A(x,\tau)=2\eta_0\,\mathrm{sech}[2\eta_0(x-\bar{x})]e^{i(vx/2+2\sigma)}\ , \tag{25}$$

with $d\bar{x}/d\tau=v$, and $d\sigma/d\tau=-v^2/8+2\eta_0^2$.

We will indicate in the second paper of this series what happens if the initial wave packet consists of several such solitons bound together. Assuming that the wave packet always resides in the left-hand medium, the perturbation term on the right-hand side of (22) will remain small, even for reasonably large nonlinear refractive-index mismatches. We can capture the effects of the interface by allowing the soliton parameters, its velocity v, and amplitude η_0 to vary slowly with τ. The basic approach presented here relies on the fact that the right-hand side of (22) is small. In this context it should be applicable in many physical situations where the NLS equation describes the evolution of some physical quantity and V represents perturbations, such as material defects, higher-order dispersion, or nonlinear terms, that could exist in the original equation but are neglected to first approximation. For example, we shall see in paper II that when V is proportional to x representing a ramped refractive-index gradient, the solution found using this approach agrees with the exact solution. The latter is obtained after a transformation that reduces the original equation to an exact NLS.[9] Another example is the evolution of temporal pulses in optical fibers where a typical V is of the form $[i\beta_1(\partial^3/\partial x^3)+\beta_2(\partial^4/\partial x^4)]+\gamma|\partial A/\partial x|^2$ (Ref. 12) and where the theory predicts that soliton pulses under this type of perturbations will decelerate at a rate proportional to the pulse width.[13] In this latter problem the x variable represents time.

This approach has also been taken for situations in which V contains terms that account for gains or losses in which p is no longer a constant. To see some examples the reader is referred to Ref. 9. Finally there is also the case of the dynamics of solitons under random perturbations where V would be a random function of x and/or τ.[14]

Going back to the problem considered here, from the conservation of power, if $A(x,\tau)$ is given by (25), then the soliton width η_0 is constant, but from Eqs. (24b) and (24c)

$$\frac{dv}{d\tau}=\frac{d^2\bar{x}}{d\tau^2}=-2p^{-1}\int_{-\infty}^{\infty}\frac{\partial V}{\partial x}AA^*dx\ . \tag{26}$$

Since AA^* is simply a function of $x-\bar{x}(\tau)$, the force on the right-hand side is a function only of $\bar{x}$ and can be written as the gradient of a potential,

$$\frac{d^2\bar{x}}{d\tau^2}=-\frac{\partial U_L(\bar{x})}{\partial\bar{x}}\ , \tag{27}$$

where $U_L(\bar{x})$ is the integral in $\bar{x}$ of the right-hand side of (26).

To determine the explicit form of U_L one has, from (23), that

$$\frac{\partial V}{\partial x}=\Delta\delta(x)+2(1-\alpha^{-1})\delta(x)|A|^2+2(1-\alpha^{-1})H(x)\frac{\partial|A|^2}{\partial x}\ ,$$

where $\delta(x)$ and $H(x)$ are the Dirac δ function and the Heaviside function, respectively; then

$$2p^{-1}\int_{-\infty}^{\infty}\frac{\partial V}{\partial x}AA^{*}dx=2p^{-1}[\Delta|A(\bar{x})|^{2}+(1-\alpha^{-1})|A(\bar{x})|^{4}] .$$

Therefore, if one defines

$$M(|A|^{2})=2\Delta|A|^{2}+2(1-\alpha^{-1})|A|^{4} ,$$

Eq. (26) becomes

$$\frac{d^{2}\bar{x}}{d\tau^{2}}=-p^{-1}M(|A(\bar{x})|^{2}) .$$

Finally, by comparing (26) and (27) one has that

$$U_{L}(\bar{x})=p^{-1}\int^{\bar{x}}M(|A(s)|^{2})ds .$$

Using the soliton expression for $A(x,\tau)$, the equivalent potential is

$$U_{L}(\bar{x})=\Delta(1-(\alpha S_{0})^{-1})\tanh(2\eta_{0}\bar{x})+(\Delta(3\alpha S_{0})^{-1})\tanh^{3}(2\eta_{0}\bar{x}) , \quad (28)$$

where S_0, the mismatch ratio is given by

$$S_{0}=\frac{1}{4(\eta_{0}/\sqrt{\Delta})^{2}(1-\alpha)} .$$

This parameter S_0, which depends on the power of the packet and on the nonlinear refractive-index mismatch, characterizes the shape of U_L, which together with the initial kinetic energy $v_0^2/2$, defines in a unique way the full evolution of the equivalent particle. The first result one can obtain from taking the first derivative of U_L,

$$\frac{dU_{L}}{d\bar{x}}=2\eta_{0}\Delta\,\mathrm{sech}^{2}(2\eta_{0}\bar{x})[1-\alpha S_{0}^{-1}\mathrm{sech}^{2}(2\eta_{0}\bar{x})] ,$$

is that a critical point of U_L ($dU_L/d\bar{x}=0$) exists only if $\alpha S_0<1$ and that it is always a maximum. If, on the other hand, $S_0\geq 1$, U_L is an increasing function of $\bar{x}$.

Equation (27) is simply Newton's second law of motion and we know that for a given set of initial conditions (position and velocity) there is a unique trajectory that the particle will follow. Typically the set of all possible trajectories is presented in a phase plane ($\bar{x}$ versus) plot, since they have an analytical expression

$$v^{2}(\bar{x})-v_{0}^{2}=2[U_{L}(\bar{x}_{0})-U_{L}(\bar{x})] ,$$

where $(\bar{x}_0,v_0)$ are the initial position and velocity of the particle. Given this, one can say that the motion of the particle and thereby the dynamics of the surface wave can be read off directly from the graphs of $U_L(\bar{x})$. Two graphs of $U_L(\bar{x})$ are drawn in Fig. 7: the first case, where $\alpha S_0<1$, shows a maximum for U_L; whereas for the case $\alpha S_0>1$ the potential is always increasing. In all cases U_L is only defined for $\bar{x}\leq 0$ since the theory was developed for the left-hand medium.

In order to start interpreting the results, let us review what the motion of the equivalent particle says about the evolution of the light beam in the dielectric. First, let us remember that the position of the particle represents the location of the beam in the medium and, if the equivalent particle approaches the position $\bar{x}=0$ with velocity v_i, this means that the beam is approaching the interface with an angle of incidence ψ_i which is proportional to $\sin^{-1}v_i$. Similarly, when the particle stops and bounces back toward $\bar{x}=-\infty$ with speed $|v_r|$, this means that the beam is reflected at an angle ψ_r proportional to $\sin^{-1}|v_r|$. Finally, if the beam crosses the interface, and this case will be discussed in Sec. IV C, and departs from it at an angle ψ_t, the equivalent particle would be in a trajectory going $+\infty$ with velocity proportional to $\sin\psi_t$.

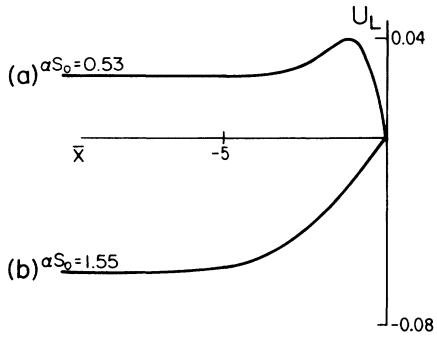

FIG. 7. Graph of $U_L(\bar{x})$ for $\alpha S_0<1$ and $\alpha S_0\geq 1$, respectively. In the first case, U_L has a maximum for some $\bar{x}<0$ and in the second case U_L is an increasing function of $\bar{x}$.

Let us start now by observing that particles initially far away from the interface but with initial velocity v_0 such that its total energy $v_0^2/2+U_L(x_0)$ is bigger than $\max(U_L)$ will cross the interface. To understand what happens in the right-hand medium we will construct a similar potential for that medium in Sec. IV B.

We can already find two global results from this part of the analysis. First, the theory shows that if $\alpha S_0\geq 1$, there are no critical points in $U_L(\bar{x})$; that is, there are no corresponding steady-state solutions in the left-hand media. On the other hand, if $\alpha S_0<1$, there is a maximum in $U_L(\bar{x})$ corresponding to the existence of an unstable steady-state surface wave centered in the left-hand medium and corresponding to the exact solution $F^{-}(x)$ in (16), which we now see is unstable. Also at the critical value $\alpha S_0=1$ the maximum is at $\bar{x}=0$ corresponding to point D in Figs. 3(a) and 3(b).

We compare the trajectories of the equivalent particle given by solving (27) with the trajectory of the peak of the self-focused channel found by numerically integrating the full equation (3). In Fig. 8 we show in a phase-plane diagram two trajectories of reflected wave packets corresponding to $\alpha=0.75$ and 0.25. We observe that the agreement between theory and the numerical simulation is remarkable, even for a larger nonlinear refractive-index mismatch. Both trajectories exhibit a large phase shift, a nonlinear analogue of the Goos-Hänchen shift. Since, as we shall see, the nonlinear Goos-Hänchen shift also exists for reflected beams that cross the interface, we will discuss this phenomenon only after considering all possible situations in Sec. IV B.

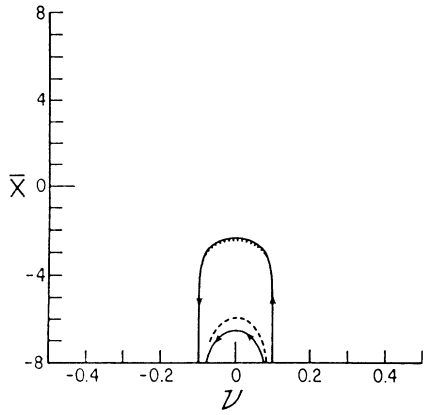

FIG. 8. Phase plane of the equivalent particle (continuous curves) corresponding to wave packets traveling in the left-hand medium at all times. Here the interface is at $\bar{x}=0$. Dotted and dashed trajectories were obtained by integrating Eq. (3) for $\alpha=0.25$ and 0.75, respectively. The value P of the incident power is 2 in both cases.

B. Self-focused channel in the right-hand medium

An exactly parallel analysis is obtained when the wave packet stays in the right-hand medium, except that, in this case, we will find that the critical point of the equivalent potential is a local maximum and therefore stable.

Let

$$F(x,z)=\left[\frac{2}{\alpha_1}\right]A(x,\tau)\exp\left[\frac{i(\beta^2-n_1^2)z}{2\beta}\right],$$

then $A(x,\tau)$ satisfies (22) with

$$V(\bar{x})=\begin{cases}-\Delta-2(\alpha^{-1}-1)|A|^2, & x<0\\ 0, & x>0\ .\end{cases}$$

If $A(x,\tau)=2\eta_1\mathrm{sech}[2\eta_1(x-\bar{x})]e^{i(vx/2+2\sigma)}$, where $d\sigma/d\tau=-v^2/8+2\eta_1^2$, the corresponding equations to (24a)–(24c) are

$$\frac{dp}{d\tau}=0\ ,$$

$$\frac{d\bar{x}}{d\tau}=v\ ,$$

$$\frac{dv}{d\tau}=-\frac{\partial U_R}{\partial\bar{x}}\ ,$$

where the equivalent potential defined for $\bar{x}\geq 0$ is

$$U_R(\bar{x})=\Delta(1-S_1^{-1})\tanh(2\eta_1\bar{x})+\frac{\Delta}{3S_1}\tanh^3(2\eta_1\bar{x})\ , \tag{29}$$

where

$$S_1=\frac{1}{4(\eta_1/\sqrt{\Delta})^2(1-\alpha)}\ .$$

We show the graph of $U_R(\bar{x})$ in Fig. 9 for three typical cases: the first one corresponds to the case $S_1>1$ and $U_R(\bar{x})$ is an increasing function of $\bar{x}$. Both 9(b) and 9(c) correspond to cases where $S_1<1$ and they show a minimum for $U_R(\bar{x})$, but in 9(c) $U_R(0)>U_R(\infty)$ and the opposite is true in 9(b). As we can see the theory predicts that above a critical power, which occurs when $S_1<1$, there is a minimum for $U_R(\bar{x})$ that corresponds to the existence of a stable steady-state solution in the right-hand medium. This solution is $F^+(\bar{x})$, given in (11) for the branch *ABC*.

So far, these equivalent potentials have given us the stability properties of branches *DE* from the potential U_L obtained in Sec. II B, and now of *ABC* of Figs. 3(a) and 3(b). At this level of approximation, the theory does not predict the existence of the solution $F^+(x)$ on branch *CD*. This is because we approximated the exact stationary solution by a soliton in order to find an explicit form of the potential. One can expect that corrections to this approximation would produce a slight change in the potential. For the purpose of the global dynamics this approximation is good enough to describe and predict the behavior for a wide range of initial conditions on the wave packet and parameters of the dielectrics. We will not attempt to construct a next-order term for the equivalent potential. Instead, we will simply argue that, based on the shape of the potentials and on numerical evidence, for powers of the wave packet corresponding to the branch *CD* of Fig. 3, the correction on U_R would be such that it would have a maximum between $\bar{x}=0$ and the position of the minimum, and that would correspond to the $F^+(x)$ solutions of that branch which therefore would be unstable.

As in the previous case, we tested theoretical trajectories with trajectories obtained from the numerical solution of Eq. (3), and in Fig. 10 we show in a phase plane two trajectories: (i) with parameters such that the equivalent potential is that of Fig. 9(a) in which case the particle approaches the interface from the right but with initial energy less than $U_R(0)$ and therefore circles the center and returns to $+\infty$ without crossing the interface,

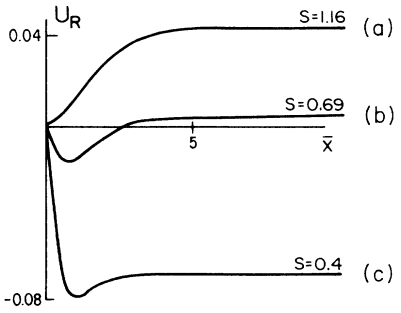

FIG. 9. Graph of $U_R(\bar{x})$ for three cases. The first one for $S_1\geq 1$ and the second and third for $S_1<1$, where there is always a minimum for some $\bar{x}>0$. In (b) $U(0)<U(\infty)$ and the opposite is true in (c).

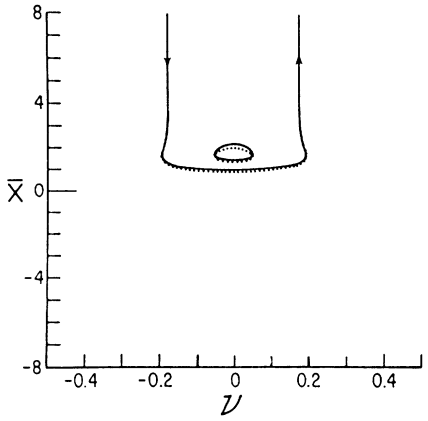

FIG. 10. Phase plane of the equivalent particle (continuous curves) corresponding to wave packets traveling in the right-hand medium at all times. Again the interface is at $\bar{x}=0$ and $\alpha=0.75$ and $P=2.0$ for both trajectories.

and (ii) a particle oscillating about the minimum of $U_R(\bar{x})$. We observe again that the agreement is excellent even in case (ii) where the wave packet stays close to the interface for all times. The numerical and theoretical trajectories remained closed even after five cycles. We note, however, that a particle with enough initial energy will cross the interface. Therefore it is clear that we need to extend the theory if we want to consider the situation in which a wave packet crosses the interface either from left to right or vice versa.

C. Transmission through the interface

If we are in the nonlinear regime shown in Fig. 6(b), then whenever the initial angle of incidence is big enough to guarantee that the wave packet will cross the interface, it will do it over an effective propagation distance of $v^{-1}\eta_0$. In most cases this distance is small and under these conditions the assumption we take is that the wave packet does not significantly change shape during the crossing. We will find that this approximation turns out to be excellent in almost all cases. However, once it has crossed it will experience the new medium with new parameters and therefore the wave packet will reshape. The theory needs to be extended to explain this behavior. The question that we need to address now is how to decompose the initial data corresponding to the wave packet in the new medium into its soliton and radiation components. We will see that if the nonlinear refractive-index ratio α is greater than $\frac{4}{9}$, then a single wave packet crossing from left to right evolves into a single wave packet with a small amount of radiation left over. If the power of the incident beam is $P_I=8\eta_0/\alpha_0$, then the power in the transmitted beam is $P_T=16\eta_0/\alpha_0(1/\sqrt{\alpha}-\frac{1}{2})$ and the power in radiation is $P_{\text{rad}}=P_I-P_T=8\eta_0/\alpha_0(1-\sqrt{\alpha})^2$. For this case, a global dynamics will now be constructed which is an extension of the theory developed in the previous subsections. We will also make a connection with the numerical results obtained in Sec. III. Contact will also be made in Sec. IV with previous work, where phenomena similar to those predicted here have been observed and left unexplained. This section ends with a definition of the nonlinear Goos-Hänchen shift which has a natural interpretation in the equivalent-particle picture.

Our earlier analysis in this section showed that, in the nonlinear regime, generically the potentials $U_L(\bar{x})$ and $U_R(\bar{x})$ have finite slopes at $\bar{x}=0$ and therefore the velocity v of the equivalent particle at the interface is finite. The crossing occurs quickly in a distance of v^{-1} times the soliton inverse with η_0. As shown by Fig. 6(b), it is only within the hornlike regions separating the nonlinear from the intermediate regimes that the crossing of the wave packet is slow enough that the assumptions made here do not apply. When the crossing time is indeed short, the wave packet does not significantly change shape during the crossing. However, once it has crossed, it will no longer be a perfect soliton of the new medium and it will consequently decompose into the normal modes associated with the new medium. We present the details of the analysis on how to determine this decomposition in paper II. However, if the nonlinear refractive-index mismatch is small enough such that $\alpha>\frac{4}{9}$, a soliton wave packet in one medium gives rise to a single-soliton wave packet in the other and very little radiation is produced at each crossing (see, for example, Fig. 11). There-

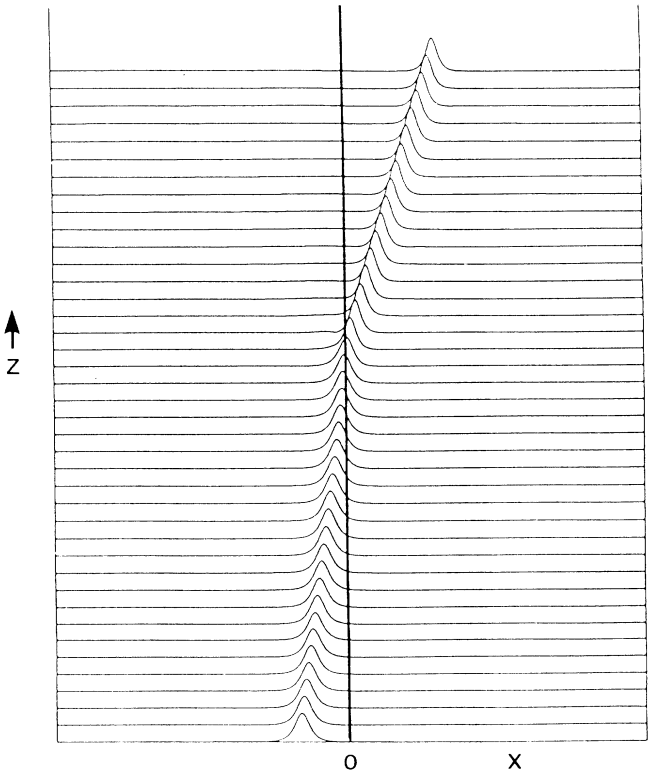

FIG. 11. Full evolution of a transmitted wave packet for $\alpha=0.75$ and $P=2.0$. The initial and final wave packets show how it reshapes in the new medium and that little radiation is produced.

fore, in this case we can construct a composite theory which describes the global dynamics of a single-soliton wave packet. To do this we simply assume no radiation losses and piece together the left- and the right-hand potentials $U_L(\bar{x})$ and $U_R(\bar{x})$ by defining the composite potential

$$U(\bar{x})=H(\bar{x})U_R(\bar{x})+[1-H(\bar{x})]U_L(\bar{x}) , \tag{30}$$

where H is the Heaviside function and $U_L(\bar{x})$ and $U_R(\bar{x})$ are given by the expressions (28) and (29) derived in the previous subsections. We emphasize that if P is the initial power of the wave packet, neglecting radiation losses effectively means that in (30) $\eta_0=\alpha_0 P/8$ in U_L and $\eta_1=\alpha_1 P/8$ in U_R, or $\eta_1=\eta_0/\alpha$, which also gives us a relation of the parameter S corresponding the right-hand medium with that of the left-hand medium, $S_1=\alpha^2 S_0$. This is a better approximation to the true values of η than keeping the same η for both U_L and U_R. To see this, we calculate the difference between $\eta_{1\,\text{exact}}=2\eta_0(1/\sqrt{\alpha}-\frac{1}{2})$ and the two possible approximations $\eta_1=\eta_0$ and $\eta_1=\eta_0/\alpha$. In the former this difference is proportional to $1-\sqrt{\alpha}$; in the latter it is proportional to $(1-\sqrt{\alpha})^2$. In (30), $U(\bar{x})$ is continuous but its derivative, the equivalent force, has a small discontinuity at $\bar{x}=0$. The motion of the particle and therefore the dynamics of the surface wave along *any* part of the waveguide can be described directly from the graph of $U(\bar{x})$ which is drawn, for all regimes in the S versus α plane, $\alpha>\frac{4}{9}$ and S corresponding to the right-hand medium in Fig. 12. In cases 12(b) and 12(c) we have a corner at $\bar{x}=0$. These regions in parameter space correspond to the interval (P_C,P_D) of Figs. 3(a) and 3(b), and, at the next order of the perturbation theory, one should find that the corner at $\bar{x}=0$ both smooths and moves slightly to the right.

We again tested our theory by comparing it with real trajectories obtained by numerically integrating the full equation (3). This comparison was comprehensive. Several comparisons of the true trajectory (formed by numerically obtaining the position of the peak and v) and the equivalent-particle trajectory were made at each of the different equivalent potential shapes. In Figs. 13 and 14, we show two potentials and phase planes: one corresponding to values of S_0 and α so that we are in region [Fig. 12(d)] of parameter space and another corresponding to region in Fig. 12(f). The two cases are important because as we show in Fig. 13(b) for a potential like that in Fig. 12(d) and Fig. 14(b) for a potential like that in Fig. 12(f), they contain all trajectory types: (1) a packet entering from the left and failing to make it over the unstable maximum, therefore ending up at $\bar{x}=-\infty$; (2) a packet entering from the left with enough energy to overcome $U_{\max}$ and end up at $\bar{x}=\infty$; (3) a packet entering from the right with enough energy to overcome $U_{\max}$, ending up at $\bar{x}=-\infty$; (4) a packet entering from $\bar{x}=\infty$, circling the center of the phase plane, and returning to $\bar{x}=\infty$. For this last trajectory, according to the theory, the packet can cross the interface twice (first from right to left, then from left to right) and (5) a packet oscillating about the stable center. For other potentials shown in Fig. 12, every beam trajectory will be similar to one of these two cases. In Fig. 15 we show the actual evolution of the wave packet corresponding to trajectory (2) of 14(b), and we can see that each time it crosses the interface it reshapes. Since radiation losses are very small, we can expect good agreement between theory and the numerical simulations and indeed from Figs. 13(b) and 14(b), we find that the agreement is excellent.

We are now in a position to explain the analytic expression that defines one of the boundaries separating the nonlinear from the intermediate regimes [Eq. (21)]. It was argued that the numerical simulations gave a value of S_0 bigger than $\max(\alpha^{-1},2/3\alpha^2)$ for all cases where the transition from intermediate to nonlinear regimes happened. What this means is that at transition in the nonlinear regime, the equivalent potential is like that of Figs.

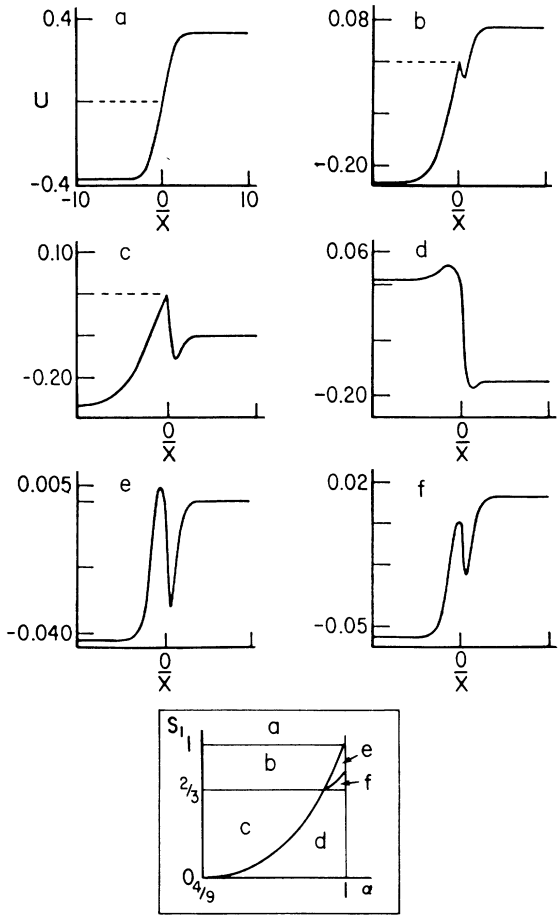

FIG. 12. Graphs of $U(\bar{x})$ for regions of different behavior in an (S_1,α) plane where $\alpha>\frac{4}{9}$. Observe that there are no stable critical points for negative $\bar{x}$. In (b) and (c) the maximum is always a corner at $\bar{x}=0$. In (d), (e), and (f) there is a maximum for $\bar{x}<0$. In (c), (d), and (e) an equivalent particle which enters from the left with enough energy to overcome the maximum will travel to $\bar{x}=\infty$ and not return. On the other hand, in (a) (b), and (f) the equivalent particle may enter the right-hand medium, remain there for a while, and eventually return to the left-hand medium.

12(a) or 12(b). In both cases there is no local maximum [although there is a corner at $\bar{x}=0$ in 12(b)] and the global maximum of U is $U(\infty)$. For each potential, the critical trajectory which separates motion ending up at $+\infty$ from that ending up at $-\infty$ gives the critical velocity of the equivalent particle (critical angle of incidence),

$$\frac{v_0^2}{2}=U(\infty)-U(-\infty)\ .$$

This condition gives, for fixed α, a relation between $v_0/\sqrt{\Delta}$ and $\eta_0/\sqrt{\Delta}$ which defines the right-hand boundary of Fig. 6(b) separating the intermediate from the fully nonlinear regimes. After substitution of $U(\bar{x})$ in this expression one obtains (21).

D. The nonlinear Goos-Hänchen shift

As was discussed briefly in the Sec. II for the linear case, it was experimentally observed[2] that a reflected wave packet suffered a shift from the position predicted by the geometrical optics approximation. For the nonlinear problem, and with the equivalent-particle description there is a natural analogue of the Goos-Hänchen shift. It is simply the difference in the asymptotic value of the z location of the equivalent reflected particle as $\bar{x}\to-\infty$ and the location of a free particle that bounces at the interface. From this definition the analytical expression for the nonlinear Goos-Hänchen shift δz is

$$\delta z=2\beta\left[\int_{-\infty}^{x_f}[v^{-1}(x)-v_0^{-1}]dx+\frac{x_f}{v_0}\right], \tag{31}$$

where

$$v^2(x)=v_0^2-2U(\bar{x})+2U(-\infty)\ ,$$

and x_f is the penetration distance, namely, the value of $\bar{x}$ at which $v_0^2=2[U(\bar{x})-U(-\infty)]=2K$. The graph of δz versus K is shown in Figs. 16(a) and 16(b); in the first

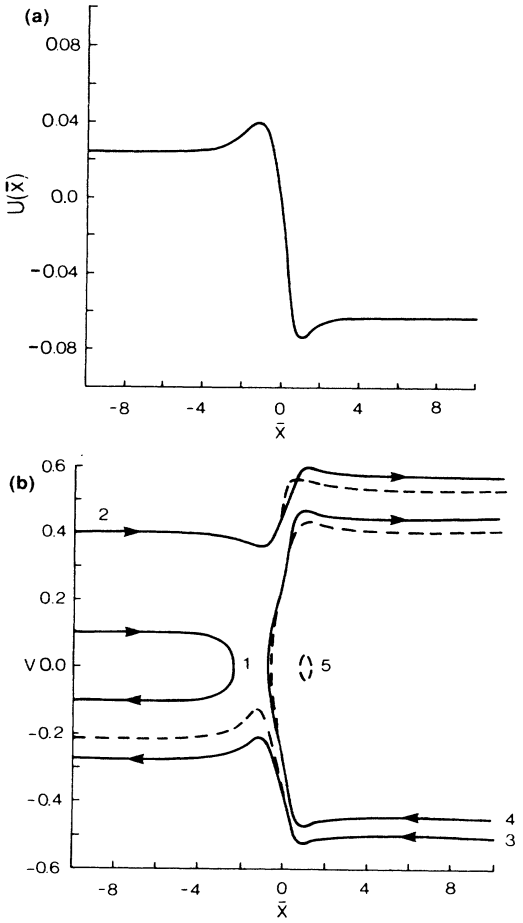

FIG. 13. Potential and phase plane for values of the parameters $\alpha=0.75$, $\Delta=0.1$, and $P=2.0$. We show all typical trajectories. Observe that the agreement is better when the wave packet does not cross the interface. This is the case for the oscillatory trajectory in the right-hand medium and the trajectory that comes from $-\infty$ and is reflected before crossing the interface.

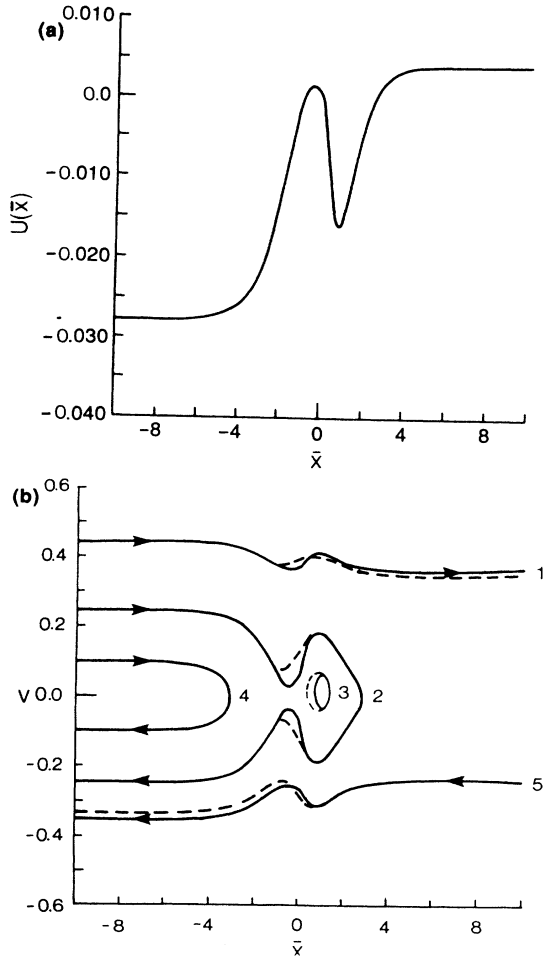

FIG. 14. Potential and phase plane for values of the parameters $\alpha=0.75$, $\Delta=0.1$, and $P=1.52$. The difference with the previous case of Fig. 13 is that now we can have a wave packet coming from $-\infty$ that crosses the interface and is reflected, ending up at $-\infty$ (trajectory 2), which is the opposite of trajectory 2 of Fig. 13.

case, which is typical for potentials with $U_{\max} < U(\infty)$, we have two singularities: a logarithmic singularity for $K_1 = U_{\max} - U(-\infty)$ which corresponds to a beam that stays trapped to the unstable NSW (in an actual experiment one would expect a large but finite nonlinear Goos-Hänchen shift with the beam being eventually reflected); the second singularity is algebraic for $K_2 = U(\infty) - U(-\infty)$, which corresponds to the critical trajectory that separates reflection from transmission. For the second type of potential where $U(\infty) < U_{\max}$, only the logarithmic singularity exists for $K = U_{\max} - U(-\infty)$.

For the particular case where $\alpha = 1$, $U(\bar{x}) = \Delta \tanh(2\eta\bar{x})$ and one can solve for δz exactly; the result is

$$\delta z = \frac{\beta}{\eta v_0}\left[\ln\left[\frac{v_0}{\sqrt{\Delta}}\right] + \frac{v_0/\sqrt{\Delta}}{[4-(v_0/\sqrt{\Delta})^2]^{1/2}}\tan^{-1}\left[\frac{v_0/\sqrt{\Delta}}{[4-(v_0/\sqrt{\Delta})^2]^{1/2}}\right]\right],$$

and in Fig. 17 we show a comparison between this expression and the resulting shift of the numerical reflected trajectories for this choice of α.

V. APPLICATIONS AND EARLIER WORK

As a simple application of the theory we illustrate in Fig. 18 how one might design an all-optical spatial scanner. In Fig. 18(a) we simply read off the channel trajectories from the phase portraits associated with the equivalent potential at the fixed power $P = 0.9$. Each trajectory corresponds to a different initial velocity (angle of incidence) of the equivalent particle (self-focused channel). Alternatively, we may fix the angle of incidence ψ_i and increase or decrease the incident channel's power. Now the shape of the equivalent potential varies slightly for an equivalent particle incident at a fixed initial velocity. This case is illustrated in Fig. 18(b). Each trajectory is obtained by decreasing the power in the incident channel by 2.5%. The numerically propagated solutions to Eq. (3) confirm the accuracy of the theory. A recent work[15] shows that the behavior described here is insensitive to the shape of the incident channel.

We have shown that the equivalent-particle theory models the numerical simulations extremely well in the cases where either (a) the wave packet stays in one medium or (b) the nonlinear mismatch α is greater than $\frac{4}{9}$. However, as we shall now see, the theory still produces a useful qualitative picture, even when the medium on the left is linear, i.e., $\alpha = 0$. This is an important case, since it has been studied previously, and in particular we now discuss the numerical results found in Ref. 3 in which a series of Gaussian wave packets is propagated from the linear medium towards the interface for a range of values of α_1.

To make contact with our theory, one can now recognize that once the packet crosses the interface in the nonlinear medium it will decompose into soliton and radiation components just as in the nonlinear-nonlinear case. The difficulty, which is only technical, is to determine what these components are. Instead, we will make the rather crude assumption that the Gaussian becomes a single soliton in the right-hand medium, with no radiation losses. Once we have a soliton in the nonlinear medium, we know that we can determine its further evolution in that medium using the equivalent-particle dynamics. To achieve this one needs to determine, for each case studied in Ref. 3, the equivalent potential in the

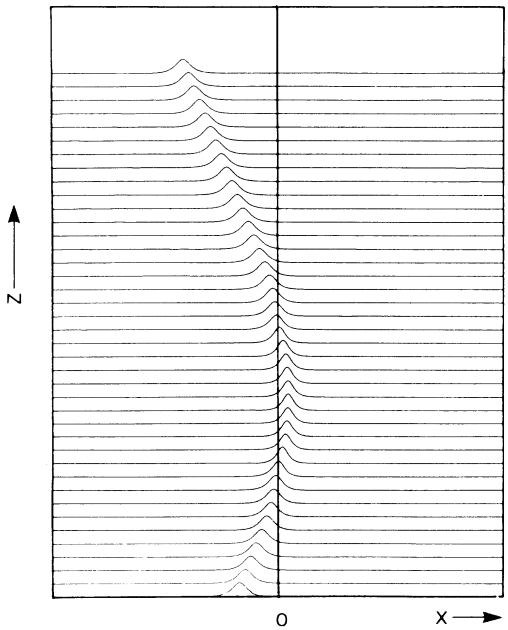

FIG. 15. Evolution of the wave packet corresponding to trajectory 2 of Fig. 14. We can see that every time the wave packet crosses the interface, it reshapes and no radiation can be detected.

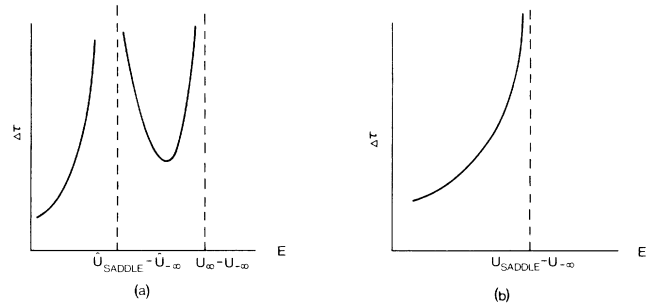

FIG. 16. Plot of $\Delta\tau = \delta z/2\beta$, the nonlinear Goos-Hänchen shift as a function of the total initial energy $E = v_0^2/2 + U(-\infty)$, of the equivalent particle. Two typical cases occur: case (a) when U is like that of Figs. 12(b) or 12(f), and (b) when U is like 12(a), (c), (d), or (e).

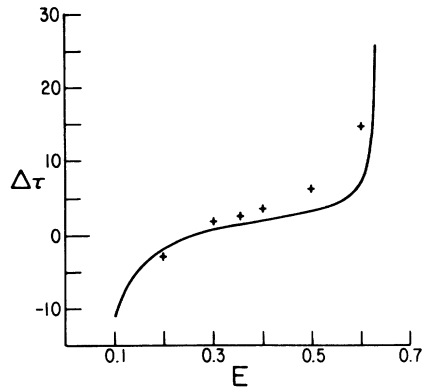

FIG. 17. Comparison between the theoretical (solid line) and the numerical (×) Goos-Hänchen shift computed from the evolution of the field in Eq. (3). Here $\alpha_0=\alpha_1=1.0$, $\Delta=0.1$, and $\eta_0=0.5$.

right-hand medium U_R and the local angle of incidence at the interface (or, equivalently, the velocity of the equivalent particle at $\bar{x}=0$). From the power of the incident Gaussian beam P_g and the nonlinear refractive-index coefficient of the right-hand medium one can compute the soliton parameter $\eta_1;\eta_1=\alpha_1 P_g/8$. This determines S_1 and thus U_R for the right-hand medium. Finally, we determine the velocity of the equivalent particle at the interface from the angle of incidence given in Ref. 3. Under the above assumptions, each beam trajectory shown in Ref. 3 corresponds, in terms of our theory, to a trajectory of the equivalent particle. Each particle will have the same initial velocity but will "see" a different potential U_R due to the changing α_1. From Fig. 9 we see that the beam is transmitted or eventually reflected back into the linear medium depending, respectively, on whether the initial equivalent particle kinetic energy $K=v_0^2/2$, which is the same in all trajectories, exceeds or is smaller than $U_R(\infty)=\Delta(1-2/3S_1)$.

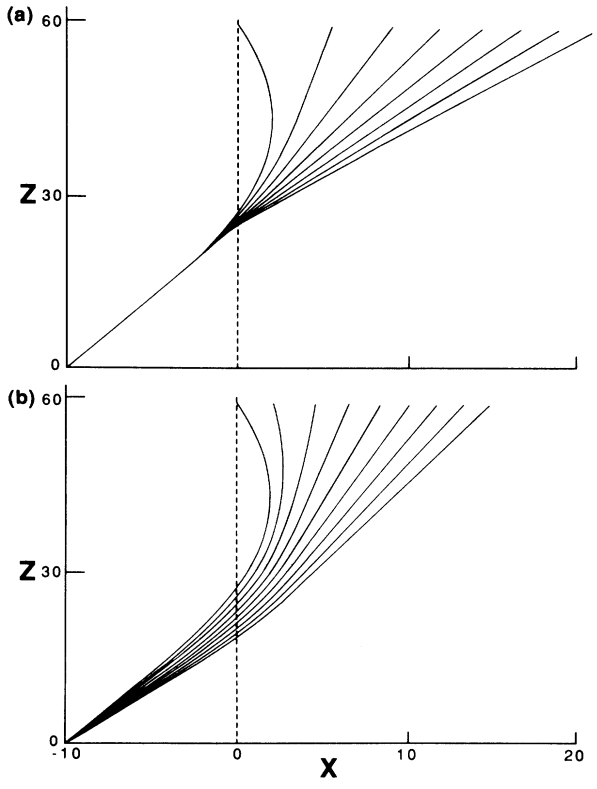

FIG. 18. A spatial scanner. In (a) we show the different trajectories of incident packets with the same incident angle but each has different power $P_i=0.4=0.025(i-1)$, $i=1,2,\ldots,8$. In (b) all incident wave packets have the same power $P=0.9$, each having a different incident angle. The equivalent-particle theory provides ways to determine where each wave packet is at the end of the device.

For the linear-nonlinear ($\alpha=0$) case

$$S_1^{-1}=4\frac{\eta_1^2}{\Delta}=\frac{\alpha_1^2P^2}{16\Delta}\ .$$

When we substitute this expression in $U(\infty)$ we have that

$$U(\infty)=\Delta\left[1-\frac{\alpha_1^2P^2}{24\Delta}\right],$$

which shows that $U(\infty)$ is a decreasing function of α_1 and $U(\infty)\rightarrow-\infty$ as $\alpha_1\rightarrow\infty$. Therefore, there is a value of α_1,α_{1c}, for which $K=U(\infty)$, and in terms of α_1, the packets will be reflected for values of $\alpha_1>\alpha_{1c}$ $[K<U(\infty)]$; for values for which $\alpha_1<\alpha_{1c}$ they will be transmitted. This is in complete agreement with the behavior of the trajectories in Ref. 3. Furthermore, using the data of that reference, we estimated the value of α_{1c} and find it to be 0.016. This is an upper bound to the value of 0.0112 found by Tomlinson *et al.* All but three curves in Ref. 3 (curves *C*, *D*, and *E*), indeed, correspond to the particle trajectories whose potentials are like that of Figs. 9(a) or 9(b). Notice that if α_1 is close to α_{1c}, the particle (the self-focused beam) stays a long time in the neighborhood of the interface and may interact strongly with it. In such circumstances, the cumulative radiation loss leads to a continual decrease of the soliton wave packet η_1 and this in turn leads to higher values of S_1. However, as S_1 increases, the potential $U_R(\bar{x})$ becomes more like Fig. 9(a) or 9(b) for which cases we know the packet is either reflected or in very special cases trapped. This scenario is in principle consistent with the three trajectories in Ref. 3 mentioned above, which the authors refer to as unexplained behavior.

We can also interpret the results of Akhmediev *et al.*[4] They did a numerical investigation of the stability properties of the stationary solutions in a linear-nonlinear case. In particular, they found a sensitive behavior when they perturbed the unstable branch (C_0B_0) of the F^+ solution close to C_0 of Fig. 4. If they chose an initial perturbation such that the power P was slightly greater than that of F^+, they found that the packet ended up at the position of a stable stationary solution. On the other hand, if the perturbed F had slightly less power than F^+, the packet was ejected into the linear medium. This sensitive behavior is a consequence of the fact that for P near C_0 in Fig. 4, the corresponding value of S_1 in the soliton

picture is close to unity, the dividing parameter between (a) and (b) in Fig. 9. Therefore, if we chose a particular F whose power is slightly greater (less) than P_0, S is less (greater) than 1. Figure 9(a) [9(b)] is obtained and the packet will move towards the stable center (will asymptote to $-\infty$).

VI. CONCLUSIONS

In conclusion, we have presented a theory which describes quantitatively the global reflection and transmission properties of a self-focused channel incident at an oblique angle to the interface separating two nonlinear dielectric media. The theory has been shown to be valid over a wide range of parameter space by extensive numerical simulation. An accurate estimate of the amount of radiation generated due to interaction with the interface has been provided. The success of the theory lies in the robustness of solitons to perturbations, allowing us to describe the light channel as a spatial soliton with slowly modulated parameters.[9] The presence of an adjoining dielectric medium serves to deflect the soliton wave packet from its otherwise rectilinear path. We have presented the nonlinear analogue of Snell's laws for propagating self-focused channels. An analytic expression for the nonlinear Goos-Hänchen shift has been derived and compares satisfactorily with full scale numerical simulations. One of the main conclusions of this part of our work is that the equivalent potential's shape depends on a general design parameter S, which is the ratio of nonlinear optical coefficients to linear refractive-index mismatch, divided by the squared power in the incident channel. If $S>1$, no equilibria exist and hence there are no trapped nonlinear surface waves. If $S<1$, an unstable equilibrium exists in the left-hand medium and a stable one in the right-hand one; this is of course dependent of the relative magnitudes of the material constants, as discussed in Sec. II. The stability of trapped nonlinear TE surface waves follows immediately from this result. Our theory provides a qualitative explanation of earlier numerical beam propagation studies at a linear-nonlinear interface.

Our discussion was limited to the parameter region $\frac{4}{9}\leq\alpha\leq 1$, where we stated that a single soliton in one medium will always remain a single soliton in the fully nonlinear regime, whether or not it crosses the interface. The reason for this is that below the critical value of $\frac{4}{9}$ the incident channel can break up into multiple self-focused channels after its peak crosses the interface. This breakup phenomenon will be a major focus of paper II which follows. The modular structure of the equivalent particle theory makes its generalization to multiple interfaces straightforward. This will be the other major topic of paper II. A preliminary report on part of the work presented here and in paper II is contained in Refs. 16.

ACKNOWLEDGMENTS

This work was carried out under the auspices of the Arizona Center for Mathematical Sciences, which is funded by U. S. Air Force Grant No. AFOSR:F49620-86-C0130. One of the authors (J.V.M.) would like to acknowledge partial support from the United Kingdom Science Research Council Grant No. GR/D/84726.

APPENDIX

Numerical techniques

The method that will be used in all numerical simulations of the nonlinear partial differential equation (3) is the split-step fast-Fourier-transform (FFT) method that was proven to be the most efficient for the case of the exact NLS.[17] The same method, or minor variations of it, has been extensively used in problems arising from other nonlinear optical phenomena.[18] We never compared this method with any other used in these type of equations because it is not the aim of this work, but we tested our code by solving the exact NLS when the initial conditions are a one- or a two-soliton state. Although we only compared our solutions with the analytical ones by simply overlapping them, we made quantitative comparisons of the first three conserved quantities of NLS, mass, momentum, and energy. Both the qualitative and quantitative comparisons showed the expected accuracy and stability of the method. For the case of Eq. (3) only the first integral $\int_{-\infty}^{\infty} FF^* dx$ is conserved, and in all simulations the error on this quantity was within 1% until some component of the field reached the numerical boundary.

We now outline the method. If we write the equation for the field $F(x,z)$ in the form

$$\frac{\partial F}{\partial z}=i(L+N)F(x,z)\ , \tag{A1}$$

where $L=\partial^2/\partial x^2$ and N are operators that represent, respectively, the linear and the remaining part of the equation. Since both L and N do not explicitly depend in z we can formally write the solution at $z+\delta z$ in terms of F at z as

$$F(x,z+\delta z)=e^{i(L+N)\delta z}F(x,z)\ , \tag{A2}$$

where the integrating operator is, from its Taylor expansion,

$$e^{i(L+N)\delta z}=I+i(L+N)\delta z+\cdots+\frac{i^n(L+N)^n(\delta z)^n}{n!}+\cdots\ . \tag{A3}$$

We approximate the operator

$$e^{i(L+N)\delta z}\sim e^{iL\delta z/2}e^{iN\delta z}e^{iL\delta z/2}\ , \tag{A4}$$

where the error is $O((\delta z)^3)$, which is obtained after Taylor expanding each operator of the right-hand side of (A4) multiplying them, and comparing the result with (A3).

What this means in terms of the error on the solution is that if $\bar{F}(x,z)$ is given by

$$\bar{F}(x,z+\delta z)=T\bar{F}(x,z)\ ,$$

where $T=e^{iL\delta z/2}e^{iN\delta z}e^{iL\delta z/2}$, then

$$|F(x,z+\delta z)-\bar{F}(x,z+\delta z)|=|e^{i(L+N)\delta z}F(x,z)-T\bar{F}(x,z)|$$
$$=|(e^{i(L+N)\delta z}-T)F(x,z)+T[F(x,z)-\bar{F}(x,z)]|$$
$$\leq|(e^{i(L+N)}-T)F(x,z)|+\|T\|\,|[F(x,z)-\bar{F}(x,z)]|$$
$$=\|T\|\,|F(x,z)-\bar{F}(x,z)|+O((\delta z)^3)\ .$$

Since $\|T\|<\infty$ by a simple induction argument, the error is

$$|F(x,z)-\bar{F}(x,z)|=O((n+1)(\delta z)^3)\ ,$$

where $z=n\delta z$. One should note that the splitting of the integrating operator presented here is different than that of Ref. 16. Effectively what this does is increase the accuracy by one order in δz.

To find $\bar{F}(x,z+\delta z)$ unde the action of the operator T is equivalent to solving first

$$\frac{\partial F_1}{\partial z}=iLF_1 \tag{A5}$$

in an interval $\delta z/2$ with initial condition $\bar{F}(x,z)$. Then solve

$$\frac{\partial F_2}{\partial z}=iNF_2 \tag{A6}$$

in an interval δz with an initial condition F_1 solution of (A5). Finally one solves (A5) again for an interval $\delta z/2$ but with initial condition F_2 solution of (A5); this will be $\bar{F}(x,z+\delta z)$. The advantage of this method is that both (A4) and (A5) are easy to solve. The solution of (A4) is found by using the Fourier transform and is given by

$$F_1=\mathcal{F}^{-1}[e^{ik^2(\delta z/2)}\mathcal{F}(F_{1\,\mathrm{in}})]\ ,$$

where $F_{1\,\mathrm{in}}$ is the initial condition and $\mathcal{F}$ is the Fourier transform. Although this is an exact solution of (A4) in the numerical scheme we use a discrete Fourier transform that introduces errors in the solution of order $O((\delta x)^n)$ where δx is the distance between points in our spatial discretization and n is the number of modes one considers in the discrete finite Fourier transform.

The solution of (A5) is simply $F_2=F_{2\,\mathrm{in}}e^{iN(|F_{2\,\mathrm{in}}|)\delta z}$, where one uses the fact that N being dependent only on $|F|$, which is z independent, is in terms of z, a constant factor in (A5).

Finally, from the solutions we will be monitoring quantities such as power, center of mass, momentum, etc., which are given in terms of spatial integrals of F and its first and second derivatives. We approximate the derivatives using forward Euler approximations, and for each integral that we compute we use the trapezoidal rule.

*Permanent address: Physics Department, Heriot-Watt University, Riccarton, Edinburgh EH14 4AS, Scotland.

[1]B. R. Horowitz and T. Tamir, J. Opt. Soc. Am. **61**, 586 (1971); Appl. Phys. **1**, 31 (1973); B. R. Horowitz, *ibid.* **3**, 411 (1974); H. K. V. Lotsch, J. Opt. Soc. Am. **58**, 551 (1968); J. W. Ra, H. L. Bertoni, and L. B. Felsen, SIAM J. Appl. Math. **24**, 396 (1973); J. Zagrodzinski, Nuovo Cimento **21B**, 129 (1974); Y. M. Anter and W. M. Boerner, Appl. Phys. **7**, 295 (1975); S. Kozaki and H. Sakurai, J. Opt. Soc. Am. **68**, 508 (1978).

[2]F. Goos and H. Hänchen, Ann. Phys. **1**, 333 (1947).

[3]W. J. Tomlinson, J. P. Gordon, P. W. Smith, and A. E. Kaplan, Appl. Opt. **21**, 2041 (1982).

[4]N. N. Akhmediev, V. I. Korneev, and Y. V. Kuz'menko, Zh. Eksp. Teor. Fiz. **88**, 107 (1985) [Sov. Phys.—JETP **61**, 62 (1985)].

[5]N. N. Akhmediev, Zh. Eksp. Teor. Fiz. **83**, 545 (1982) [Sov. Phys.—JETP **56**, 299 (1982)]; C. T. Seaton, J. D. Valera, R. L. Shoemaker, G. I. Stegeman, J. T. Chilwell, and S. D. Smith, IEEE J. Quantum Electron. **QE-21**, 774 (1985); G. I. Stegeman, J. Ariyasu, C. T. Seaton, T. P. Shen, and J. V. Moloney, Appl. Phys. Lett. **47**, 1254 (1985); special issue on nonlinear waveguides [J. Opt. Soc. Am. B **5** (1988)], and references therein.

[6]C. K. R. T. Jones and J. V. Moloney, Phys. Lett. **117A**, 175 (1986).

[7]M. Grillakis, J. Shatah, and W. Strauss, J. Functional Anal. **74**(1), 160 (1987).

[8]J. V. Moloney, J. Ariyasu, C. T. Seaton, and G. I. Stegeman, Appl. Phys. Lett. **48**, 826 (1986); L. Leine, Ch. Wächter, U. Langbein, and F. Lederer, Opt. Lett. **11**, 590 (1986).

[9]D. J. Kaup and A. C. Newell, Proc. R. Soc. London, Ser. A **361**, 413 (1978).

[10]A. A. Maradudin, *Surface Waves in Modern Problems of Surface Physics*, edited by I. J. Lalov (Bulgarian Academy of Sciences, Sofia, 1981), pp. 11–399.

[11]A. E. Kaplan Zh. Eksp. Teor. Fiz. **72**, 1710 (1977) [Sov. Phys.—JETP **45**, 896 (1977)].

[12]Y. Kodama and A. Hasegawa, IEEE J. Quantum Electron. **QE-23**, 510 (1987).

[13]Y. Kodama and K. Nozaki (unpublished).

[14]Y. S. Kivshar, A. M. Kosevich, and O. A. Chubykalo, Phys. Lett. **125A**, 35 (1987).

[15]P. Varatarajah, J. V. Moloney, and A. B. Aceves (unpublished).

[16]A. B. Aceves, J. V. Moloney, and A. C. Newell, J. Opt. Soc. Am. B **5**, 559 (1988); Phys. Lett. **129A**, 231 (1988).

[17]T. R. Taha and M. J. Ablowitz, J. Comput. Phys. **55**, 203 (1984).

[18]A. Hasegawa and F. D. Tappert, Appl. Phys. Lett. **23**, 142 (1973); **23**, 171 (1973); J. A. Fleck, J. R. Morris, and E. S. Bliss, IEEE J. Quantum Electron **QE-14**, 353 (1978).